IEEE Robotics and Automation Letters (RA-L) paper, presented at ICRA 2026, Vienna, Austria. Cite as RA-L paper.

Bundled Liquid Crystal Elastomer Actuators with Integrated Cooling for Mesoscale Soft Robots

Anoush Sepehri, Sukjun Kim, *Member, IEEE*, Devyansh Agrawal, Hannah Yared, Gaoweiang Dong, Shengqiang Cai, and Tania K. Morimoto, *Senior Member, IEEE*

***Abstract*—Liquid crystal elastomer (LCE) is a promising material to develop thermally-driven soft actuators due to its high force density, large elastic strain limit, and mechanically programmable nature. However, the complex trade-off between the force generated and the response speed (i.e., cooling rate), along with the lack of systematic design guidelines necessary to design such actuators using LCE, has significantly limited its widespread adoption for soft robotic applications at the mesoscale (cm-scale). In this work, we developed thermally-driven soft actuators by bundling LCE units with integrated cooling that increased the response speed by over 400% when compared to relying only on passive cooling. We developed and experimentally validated an electro-thermo-mechanical model to predict the force and cooling rate of our actuator and established systematic design guidelines to build our actuators for different soft robotic applications. Using our proposed guidelines, we present an inchworm inspired locomotion robot with a top speed of 6 body lengths per minute. We also present a textile forearm cuff with integrated haptic feedback that can provide up to 4 mm of skin stretch feedback with a cooling rate of 1 second. Overall, the presented actuator, experimental results, and design guidelines expand the potential use cases for thermally-driven actuators in soft robotic applications at the mesoscale.**

***Index Terms*—Soft Robot Materials and Design, Soft Robot Applications, Liquid Crystal Elastomer, Soft Actuators**

I. Introduction

SOFT robotics, and particularly the development of soft actuators, has garnered considerable interest due to their unique ability to achieve safe, adaptive, and biomimetic motions. Researchers have developed many different types of soft actuators that combine expertise in material science and engineering. Soft fluidic actuators are among the most common class of actuators used in soft robotics [1]. They consist of an anisotropic enclosure made from elastomers [2] or textiles [3], and can generate complex motions when pressurized by a fluid. While these actuators can generate large forces and have sufficient bandwidth for many applications, they require bulky back-end equipment, such as large volumetric flow pumps and pressure regulators. These components ultimately limit the portability of these actuators, introducing new challenges for wearable devices (i.e., assistive robots or haptic interfaces) and mobile robots that must be ungrounded for practical use.

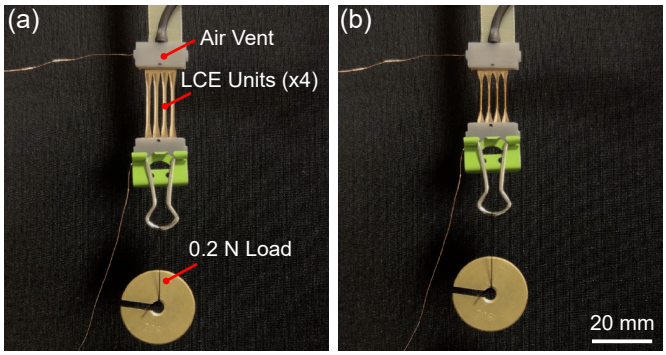

Fig. 1. Example of our thermal actuator in (a) the relaxed (cooled) state and (b) the contracted (heated) state, lifting a 20 gram load by approximately 4 mm. The actuator consisted of LCE units bundled in parallel with integrated cooling using forced convection from an air vent.

Thermal actuators are another class of soft actuators that do not inherently require bulky and complex control hardware for operation. They can generate force and motion due to thermal expansion or change of phase when exposed to different temperatures. One of the most common types of materials used to develop thermal actuators is shape memory alloys (SMA). While SMA have very high force density and are easy to actuate, they typically have one way shape memory and small elastic strain limits (5%) in their uncoiled configuration [4]. Liquid crystal elastomer (LCE) is an emerging type of soft material that, when heated, can change from a nematic state (relaxed) to an isotropic state (contracted). LCE has a number of advantages over SMA when used as an actuator: they have two way shape memory, are softer and more compliant, and have a larger elastic strain limit during actuation ($> 40\%$).

While SMA and LCE are both promising materials to develop thermal actuators, there are a number of challenges that limit their widespread adoption. In particular, thermal actuators have a relatively long response time due to the cooling rate of the material [5]. As a result, robots and devices that use thermal actuators are generally slow, with cooling rates in the tens of seconds and, in some cases, minutes [6]–[14]. To address this challenge, researchers have developed SMA and LCE actuators at the microscale to reduce the thermal inertia of the material and successfully achieved bandwidths in the tens of hertz [15], [16]. Minimizing the mass of the actuator,

Manuscript received: March 19, 2025; Accepted May 30, 2025

This paper was recommended for publication by Cecilia Laschi upon evaluation of the Associate Editor and Reviewers' comments.

This work was supported in part by the Arnold and Mabel Beckman Foundation. (Corresponding author: Tania K. Morimoto)

Anoush Sepehri, Sukjun Kim, Devyansh Agrawal, Shengqiang Cai, and Tania K. Morimoto are with the Department of Mechanical and Aerospace Engineering, University of California, San Diego, CA 92093 USA (e-mail: asepehri@ucsd.edu; suk056@ucsd.edu; dagrawal@ucsd.edu; s3cai@ucsd.edu; tamorimoto@ucsd.edu)

Gaoweiang Dong is with the Materials Science and Engineering Program, University of California, San Diego, CA 92093 USA (e-mail: gadong@ucsd.edu)

Hannah Yared is with the Department of Mechanical and Aerospace Engineering, University of California, Los Angeles, CA 90095 USA (e-mail: hannahyared@g.ucla.edu)

Digital Object Identifier (DOI): see top of this page.

IEEE Robotics and Automation Letters (RA-L) paper, presented at ICRA 2026, Vienna, Austria. Cite as RA-L paper.

however, reduced the maximum force generated, thus limiting the proposed actuators to microscale applications. In general, there is a complex trade-off between force output and response speed that currently limits the suitability of these thermal actuators for soft robots and applications at the mesoscale.

While the vast majority of robots using thermal actuators rely on passive cooling [5], some groups have investigated active cooling methods to improve the response speed. One method is to heat and cool the actuators by injecting hot and cold liquids through the material [17] or by submerging the actuator in a liquid coolant [18], [19]. Both approaches, however, require large and cumbersome equipment to store and regulate the liquids. Forced air convection has shown promise for improving the response speed of SMA actuators [20], however, existing work required large flow rates (>24 LPM) to get considerable cooling effects, likely due to the length of the actuator and parallel flow configuration.

In this work, we developed a new thermal actuator using LCE that minimizes the trade-off between force output and response speed commonly seen in existing literature. We bundled LCE units in parallel to increase the surface area of the actuator in order to offset the increase in thermal inertia needed to generate high forces (see Fig. 1). We also integrated active cooling by using a low-profile air vent to generate cross flow over the LCE units to increase the rate of heat dissipation. Furthermore, we developed an analytical model that considers both the force and response speed of the LCE units to provide systematic guidelines to design our actuators for different soft robotic applications.

To highlight how our actuator can be used for applications where both high force and high bandwidth are beneficial, we designed an inchworm-inspired locomotion robot and a textile forearm cuff with integrated haptic feedback using our design guidelines. The results and conclusions made in this work not only address the traditional force-speed trade-off for thermally-driven soft actuators, but also provide a new type of thermal actuator with relevant design guidelines to enable their use in diverse soft robotic applications.

II. Material and Methods

A. Motivation

The response speed of a thermal actuator is dependent on the heating and cooling rates of the material. For Joule heating, the time to heat the actuator can be precisely controlled by tuning the applied power. Previous work has demonstrated actuation speeds as fast as 13.5 ms by applying high power for short periods [21]. The cooling rate of the actuator, however, is dependent on the thermal properties of the material and the environment, which are harder, and in some cases impossible, to control. As a result, we focused on improving the cooling rate of our thermal actuator to improve the overall speed.

The cooling rate of a thermal actuator, assuming lumped thermal capacitance, is governed by the following equation.

$$\frac{\delta T}{\delta t} = \frac{1}{mC}(hA(T - T_\infty)) \tag{1}$$

m and C represent the mass and specific heat capacity of the material, T_∞ represents the temperature of the environment, A represents the surface area of the actuator, and h represents the convective heat loss coefficient. The first order differential equation has the following solution:

$$T(t) = T_\infty + C_1 e^{-t/\tau} \tag{2a}$$

$$\tau = \frac{mC}{hA} \tag{2b}$$

C_1 is a constant determined by initial conditions, and τ is the time constant that determines the cooling rate of the actuator. Assuming the specific heat capacity of the material cannot be changed, one can increase the response speed of the actuator without changing the force output (i.e., not reducing the mass) in two ways: (1) increase the surface area (A) of the actuator, or (2) increase the convective heat loss coefficient (h). These two observations provide the basis for the design decisions we made when developing our actuator.

To increase the surface area of the thermal material exposed to the environment, we bundled several LCE units in parallel. We hypothesized that bundling several thinner LCE units together would increase the rate of heat dissipation, while still achieving a force output similar to that of a single, thicker LCE unit with equivalent cross sectional area. Previous work has investigated looping SMA wires to work mechanically in parallel and has shown promise in increasing the force without sacrificing actuation frequency [22], [23].

To increase the rate of heat dissipation without significantly increasing the complexity of our actuators, we used forced air convection by integrating an air vent into our actuator. The vent consisted of a single air duct angled at 10° to generate cross flow over the LCE units (see Fig. 1). Although introducing any form of active cooling would increase the complexity of our actuator, our air vent was small enough that we could generate sufficient flow velocities at low volumetric flow rates (<5 LPM for all experiments in this work) that can be achieved using small portable air pumps in the future.

B. Fabricating LCE Units

We synthesized the LCE pre-cursor solution using the procedure and chemical composition described in previous work [24]. We maintained a stoichiometry of $2n_{C6BAPE}$: $3n_{TAC}$: $4n_{PETMP}$: $2n_{EDDET}$ = 0.9:0.1:0.5:0.5, for LCE synthesis. To fabricate the loosely cross-linked LCE, we employed a compression assisted molding technique (see Fig. 2a(i)) to control the thickness of the LCE films [21], [24]. For LCE films greater than 100 µm, we used commercially available PTFE tapes as spacers between the glass plates. For LCE films thinner than 100 µm, we varied the applied compression on the glass plates without any spacers.

After the loosely cross-linked LCE was removed from the glass slides, the material was laser-cut into LCE units that were dog-bone shaped with a gauge length of 10 mm and gauge width of 2 mm (see Fig. 2a(ii)). The shoulders of the dog-bone were kept several millimeters wider than the gauge width to minimize heating at the ends of the LCE units that were attached to the electrodes. The LCE units were stretched to twice the original length of the gauge section ($\lambda = 2$) and exposed to UV light (365 nm) for 60 minutes to obtain the

IEEE Robotics and Automation Letters (RA-L) paper, presented at ICRA 2026, Vienna, Austria. Cite as RA-L paper.

monodomain LCE sample (see Fig. 2a(iii)). We then sputter deposited 5 nm of Cr and 40 nm of Au on one side of the LCE units to create an electrically conductive film for Joule heating (see Fig. 2a(iv)). When fabricating the LCE units in the bundled configuration, we laser cut an array of LCE units in a single piece to simplify the manufacturing process.

C. Actuator Design and Control

Each actuator consisted of two end caps that held the LCE units in parallel (see Fig. 2b). The end caps were fabricated using general purpose resin (Grey Pro Resin, Formlabs) on a Stereolithography 3D printer (Form 3, Formlabs). One end cap included the vent to generate cross flow over the LCE units. We first laser cut and attached a fiber-reinforced epoxy laminate (FR4) plate to the ends of the LCE units using electrically conductive Z-tape (9703, 3M). We covered the FR4 with conductive copper tape and soldered copper wire directly onto the FR4 to attach to the electronics that controlled the power supplied to the LCE units. Lastly, we attached the FR4 plates to the end caps using double sided adhesive (9495LE, 3M). We attached the air vent to a one-way valve (GVP-211C-12D, Automation Direct) that was connected to an external pressure source for active cooling.

When heating the actuator, the power supply was turned on and the valve was closed, corresponding to the contracted state (see Fig. 1a). We varied the applied voltage and used a current sensor (4226 INA260, Adafruit) to estimate the power supplied during heating. When cooling the actuator, the power was turned off and the valve was opened, corresponding to the relaxed state (see Fig. 1b). We used a microcontroller (Arduino UNO, Arduino) to control two MOSFETS that turned the power supply and valve on and off. Importantly, our active cooling strategy could be turned off when heating the actuator, therefore minimizing energy consumption and avoiding high power/current requirements seen in previous work [18], [19].

D. Electro-Thermo-Mechanical Modeling

We developed an analytical model to predict the temperature, blocked force, and cooling rate for a single LCE unit given the input power. We modeled the LCE unit as a lumped capacitance system and took into account the power supplied by Joule heating and thermal losses due to convection and radiation as seen in Eq. 3.

$$\frac{\delta T}{\delta t} = \frac{1}{mC}(\eta P_{in} - hA(T - T_\infty) - (eA + e_{au}A_{au})\sigma_{bo}(T^4 - T_\infty^4)) \tag{3}$$

P_{in} represents the supplied power, m, C, T_∞, and h are defined as in Eq. 1, σ_{bo} represents the Boltzmann constant, e_{au} represents the emissivity coefficient of the gold, A_{au} represents the surface area that was covered with gold, e represents the emissivity coefficient of the LCE, and A represents the surface area not covered in gold. We assumed that the temperature of the environment (T_∞) was 25°C and constant. The density of the LCE was 1200 kgm^{-3} and the specific heat capacity was 1655 Jkg^{-1}K^{-1} based on experimental measurements. We approximated the emissivity coefficient for the LCE and gold to be 0.95 and 0.05, respectively [25]. We also estimated that only 90 % of the supplied power was used to heat the LCE units ($\eta = 0.9$) based on measurements of the resistance in the copper wire and contact resistance between the electrodes and gold film.

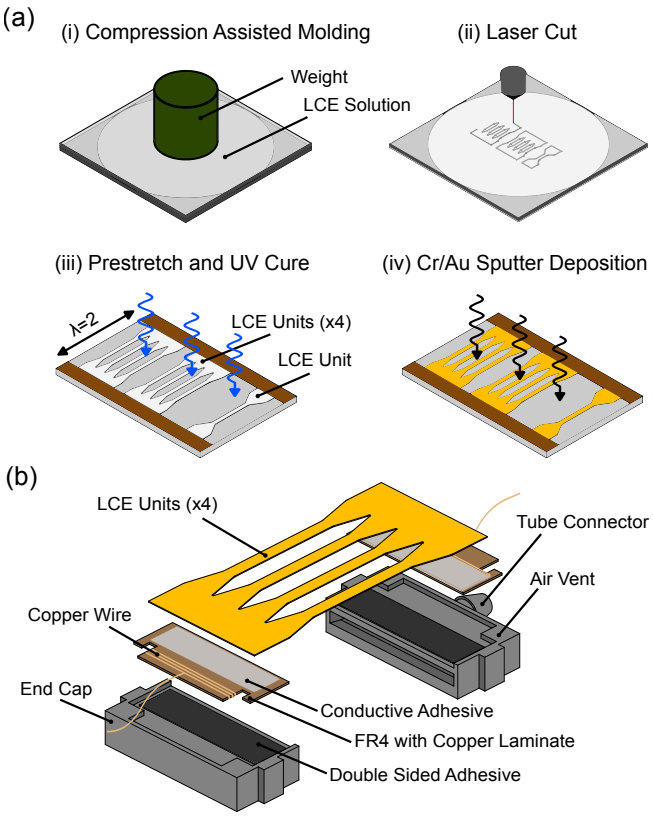

Fig. 2. (a) Steps to fabricate the LCE units: (i) We used compression assisted molding to create the loosely cross-linked LCE. (ii) We laser cut the loosely cross-linked LCE into LCE units. (iii) We stretched the LCE units before the final curing. (iv) We applied a layer of chromium and gold directly onto one surface of the LCE units to create a thin conductive film for heating. (b) Exploded view of the thermal actuator with four LCE units bundled together.

To estimate the heat loss coefficient for free convection (i.e., passive cooling), we modeled the LCE as a thin horizontal wire by calculating the equivalent diameter of the cross section when assuming the perimeter was constant. Using this approximation, we can calculate the Nusselt number (Nu) using the correlation by Churchill *et al.* [26] and the corresponding Rayleigh (Ra) and Prandtl (Pr) numbers as follows:

$$Nu = 0.36 + 0.518\left(\frac{Ra}{(1 + (0.559/Pr)^{\frac{9}{16}})^{\frac{16}{9}}}\right)^{\frac{1}{4}} \tag{4}$$

We approximated the film temperature around the LCE unit to be 62.5°C to determine the thermal properties of the air in order to calculate the Rayleigh and Prandtl numbers. Using the Nusselt number, we estimated the heat loss coefficient as:

$$h = Nu\frac{k}{D} \tag{5}$$

where k is the thermal conductivity of the air at the film temperature, and D is the equivalent diameter of the LCE unit. To estimate the heat loss coefficient for forced convection, we once again modeled the LCE as a thin horizontal wire. We

IEEE Robotics and Automation Letters (RA-L) paper, presented at ICRA 2026, Vienna, Austria. Cite as RA-L paper.

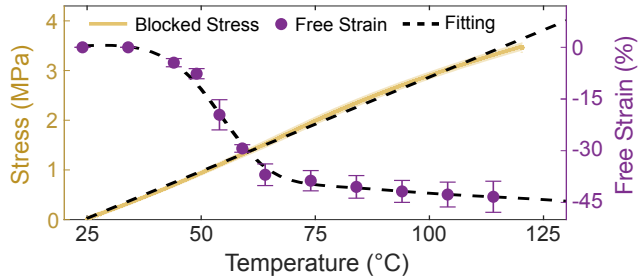

Fig. 3. Blocked stress and free strain characterization of the LCE used in this work. All experiments were repeated three times. Error bars and shaded regions indicate the standard deviation of the free strain and blocked stress measurements, respectively.

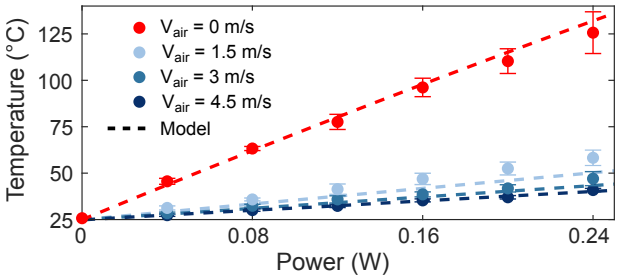

Fig. 4. Temperature of the LCE unit versus electrical power and flow velocity out of the air vent. All experiments were repeated three times and include standard deviation error bars.

used another correlation by Churchill *et al.* [27] that provided estimates of the Nusselt number for thin wires in cross flow:

$$Nu = 0.3 + 0.62 \frac{Re^{\frac{1}{2}} Pr^{\frac{1}{3}}}{(1 + (0.4/Pr)^{\frac{2}{3}})^{\frac{1}{4}}} \tag{6}$$

To calculate the Reynolds Number (Re), we assumed uniform air velocity around the LCE units, which we estimated based on the volumetric flow rate and cross sectional area of the vent. We then calculated the heat loss coefficient using Eq. 5.

For any power P_{in}, we can solve Eq. 3 to predict the temperature of the LCE unit as a function of time. To estimate the force, we mapped the temperature of the LCE to the blocked stress using experimental data (see Section III and Fig. 3). We then estimated the force based on the cross sectional area of the LCE unit.

III. Characterization Results

A. LCE Material Characterization

We first measured the blocked stress and actuation strain in the free standing state of the LCE at different temperatures (see Fig. 3). We tested three samples up to 120°C using a dynamic material analyzer (RSA-G2, TA Instruments). To measure the blocked stress, we swept through the temperature at a rate of 10°C/min. To measure the actuation strain, we manually set the temperature at fixed increments and modified the gap length between the clamps holding the LCE until the force was zero. The change in gap length then corresponded to the strain. Our LCE generated approximately 3.5 MPa of stress at 120°C and over 40% strain, with the majority of the strain occurring at the phase transition temperature (55°C).

B. Active versus Passive Cooling

To evaluate the effectiveness of our active cooling strategy, we characterized the temperature of the LCE units at steady state as a function of input power with forced convection at different flow velocities. We varied the input power to a single LCE unit up to a maximum of 0.24 W and measured the steady-state temperature using a thermal IR camera (One Edge Pro, Flir). We tested three LCE units that were on average 22 mm long, 1.3 mm wide, and 104 µm thick. We heated the LCE unit while the vent was opened with flow velocities up to 4.5 m/s (see Fig. 4). We estimated the velocity by measuring the volumetric flow rate using a flowmeter (FMA-1611A-V2, Omega) and assumed uniform flow out of the vent.

Even for small flow velocities (1.5 m/s) the steady state temperature was reduced by over 50% when compared to the passive cooling (0 m/s) configuration, suggesting that forced air convection can be an effective means to increase the rate of heat dissipation of the thermal actuator. We did not exceed 0.24 W because we observed non-uniform heating, likely due to the gold film becoming damaged from the high temperatures in the passive cooling configuration. For the remainder of the experiments, we set the flow velocity out of the air vent to 3 m/s because we observed diminishing improvements in heat dissipation for higher flow rates. In our analytical model, we assumed uniform cross flow over the LCE unit, however, variations in cross flow due to the position of the air vent and non-uniform flow velocity likely led to the minor discrepancy between the model and experimental results.

C. Blocked Force Characterization: Single LCE units

We first characterized the force generated by a single LCE unit ranging from 25 µm to 219 µm thick under isometric conditions at 0% strain (see Fig. 5a). We applied up to 0.24 W of power to each sample and measured the steady state force using the dynamic material analyzer. Each LCE unit was 1.3 mm wide and approximately 22 mm long. As expected, the thicker LCE units were capable of generating considerably larger forces and could reach over 0.6 N at maximum power.

We then measured the rate of cooling for the different LCE units when a square wave input was applied to quantify the trade-off between force output and response speed (see Fig. 5b). We applied a 0.12 W square wave input and defined the cooling time as the time it took for the blocked force to decrease from 90% to 10% of its maximum value (see Fig. 5c for representative results). We set the period of the square wave to be considerably longer than the expected cooling time to ensure the force would converge to the steady state values. We measured the cooling time manually during post processing analysis and estimated the predicted cooling time from our analytical model by numerically simulating the step response. When the thickness of the LCE units increased, the cooling time increased accordingly. For passive cooling, the cooling rates of the LCE units ranged from 1.83 seconds for the 25 µm thick samples, to over 16 seconds for the 219 µm thick samples. In contrast, the cooling rates in the active cooling configuration were over 400% faster, ranging from 0.35 seconds to 4 seconds, thus significantly increasing the response speed.

IEEE Robotics and Automation Letters (RA-L) paper, presented at ICRA 2026, Vienna, Austria. Cite as RA-L paper.

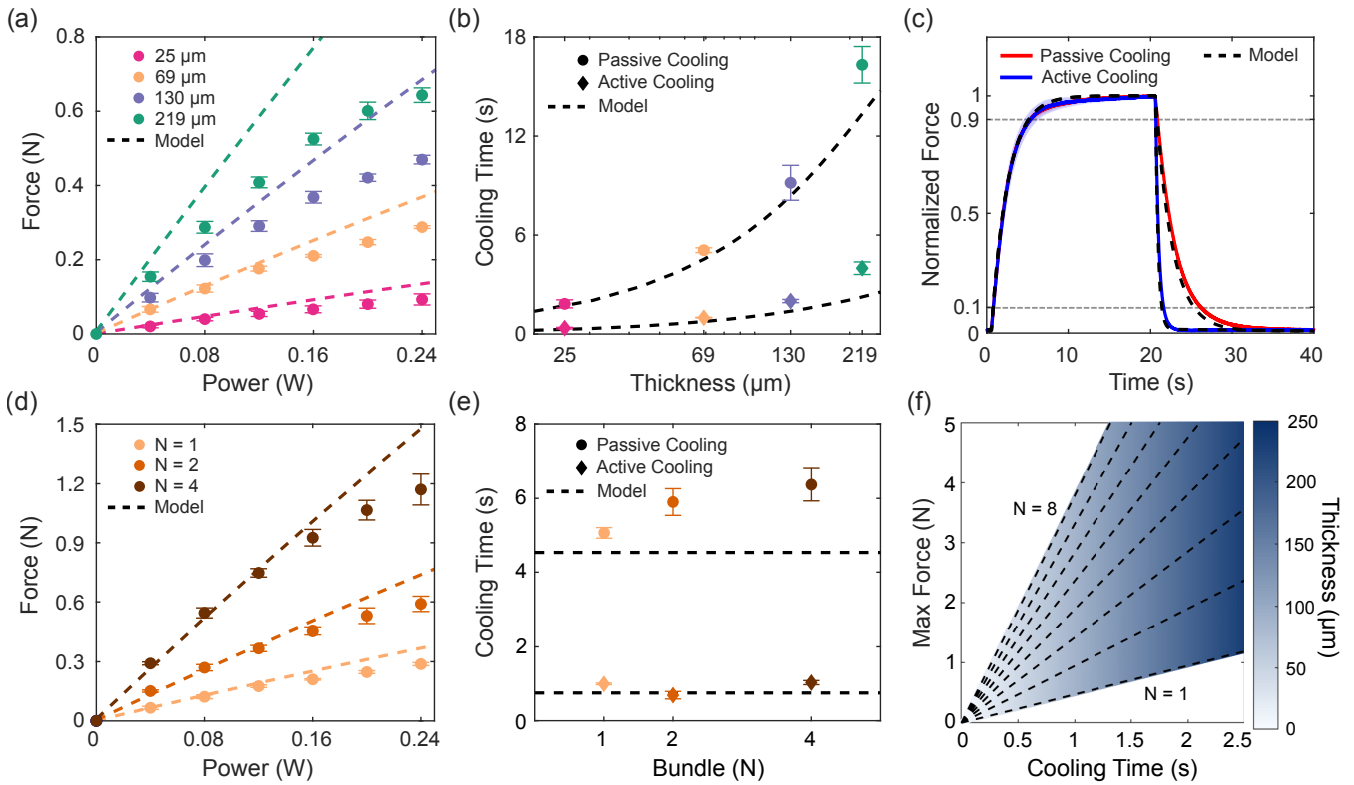

Fig. 5. (a) Steady state force generated by a single LCE unit. (b) Cooling rate of a LCE unit for the passive and active cooling configurations. (c) Representative results of the step response for a 69 µm thick LCE unit (normalized). (d) Steady state force generated by LCE units (69 µm thick) bundled together (n = 2 and n = 4). (e) Cooling rate of the bundled LCE units in the passive and active cooling configurations. All experiments were repeated three times. Standard deviation of our measurements were represented by the error bars or shaded regions. (f) The design contour based on our analytical model to select the thickness and number of LCE units to bundle together. See Section IV for examples of how the design contour can be used for different applications.

While our analytical model could accurately predict the blocked force and cooling rates for thinner LCE units, it showed larger errors for greater thicknesses. We believe this is primarily because our assumption that the LCE units can be modeled as a lumped capacitance system holds less for thicker LCE units. Additionally, we believe that larger shear stresses between the gold film and Z-tape likely caused micro-fractures in the gold that increased the contact resistance when heating, therefore reducing the overall force output.

D. Blocked Force Characterization: Bundled LCE units

We characterized the blocked force generated by a bundle of LCE units to investigate how bundling impacts the total force output and overall cooling rate of our actuator (see Fig. 5d and Fig. 5e). We bundled 2 LCE units and 4 LCE units together, all 69 µm thick to fall within the range of thicknesses tested in our previous experiments. By bundling LCE units together, we can operate them mechanically in parallel to multiply the force output (see Fig. 5d). We observed, however, that the passive cooling rates increased when more LCE units were bundled together (see Fig. 5e). We believe this was because as the LCE units cooled, they increased the temperature of the surrounding environment, thus reducing the cooling rates of the neighboring LCE units. For the active cooling configuration, we observed no increase in cooling rate. We believe this was because the fluid flow from the air vent provided effective heat transport to keep the air around the LCE units near room temperature.

E. Actuator Efficiency Evaluation

For a single LCE unit with a representative thickness of 50 µm, we estimated the energy efficiency when lifting a constant load based on our analytical model and material characterization results. We estimated the energy required to heat the LCE unit up to 120°C in 0.1 seconds and assumed a linear relationship between the force and displacement. With these assumptions, we calculated a maximum efficiency of 0.15% when lifting a load of approximately 11 grams. While our actuator has low energy efficiency, it is within the typical range for thermal actuators ($< 2\%$) that are influenced by free convection to ambient air during the heating phase [28].

F. Design Contour for Fabricating Actuator Bundles

Our modeling and characterization results quantified the trade-off between the maximum force and overall responsiveness of the LCE units that must be considered when designing our actuator for a given application. Using our analytical model, we propose a design contour (see Fig. 5f) that can aid in selecting the thickness and number of LCE units to bundle into an actuator, given force and speed requirements. While the design contour shown here is applicable for a flow velocity of 3 m/s, new contour plots can be generated for different flow velocities using our analytical model. Each dashed line corresponds to a different number of LCE units (shown up to 8 for clarity) bundled together. The thickness is specified based on the color of the contour. Consequently, each point on the dashed lines corresponds to an actuator configuration, defined

IEEE Robotics and Automation Letters (RA-L) paper, presented at ICRA 2026, Vienna, Austria. Cite as RA-L paper.

by the thickness and number of LCE units bundled together, that is theoretically capable of achieving the force and cooling rates specified by the axes. Using our design contour, force and cooling requirements can be overlayed to eliminate regions of the contour that would result in actuators that are not suitable. Examples of how the design contour can be used for different robotic applications are highlighted in the next section.

IV. Application Studies and Demonstrations

Here we present two applications in robotics and haptics at the mesoscale that can benefit from our thermal actuator and design guidelines: (1) an inchworm-inspired locomotion robot, and (2) a wearable textile cuff that can generate continuous haptic feedback on the forearm.

A. Inchworm Inspired Crawling Robot

There has been extensive research to design locomotion robots using thermally-driven actuators, however, their speeds are generally limited ($<$ 0.21 body lengths per minute (BL/min)) due to the cooling rates of the actuator [8]–[12]. We designed a 44 mm long crawling robot with the goal of surpassing the top speeds achieved by existing locomotion robots using thermally-driven actuators.

1) Inchworm Robot Design: Our robot consisted of two 3D-printed end mounts that held the feet, thermal actuator, and flexure-based linear spring (see Fig. 6). As the actuator was heated and cooled, a cyclic motion was generated that resulted in forward linear motion due to the anisotropic friction between the feet and the ground. The feet were made from 100 µm thick FR4 that was attached at a 60° angle relative to the horizontal plane. We determined during preliminary experiments that knitted fabric was a suitable medium for the robot to move on to maximize the anisotropic friction between the ground and the feet. We also constrained the robot to linear motion by including a guide rail made from a kapton tube that the robot could slide along. We created the linear spring by laser cutting a 3 mm wide piece of FR4 (200 µm thick) before attaching it to the end mounts (see Fig. 6b). When the actuator was placed onto the end mounts, the spring was compressed by approximately 7 mm due to the passive stiffness of the LCE units. We introduced some preload on the spring to ensure the restoring force could overcome the static friction between the feet of the crawler and the ground.

To design our thermal actuator for the inchworm robot, we aimed for a stride length of 5 mm within 0.1 seconds of heating and a cooling rate of 0.5 seconds, achieving a theoretical top speed of 8.33 mm/s, or over 10 BL/min based on the robot's length (44 mm). We estimated the necessary blocked force of our actuator to achieve the desired stride length using Eq. 7.

$$k\delta x + F_{load} = F_b\left(1 - \frac{\epsilon}{\epsilon_m}\right) \tag{7}$$

δx represented the desired stride length (5 mm), ϵ represented the contraction ratio of the LCE units, and ϵ_m represented the maximum contraction ratio of the LCE in free space ($\epsilon_m = 0.43$, see Fig. 3). We estimated the spring constant of the flexure spring, k, to be 0.0103 N/mm by conducting

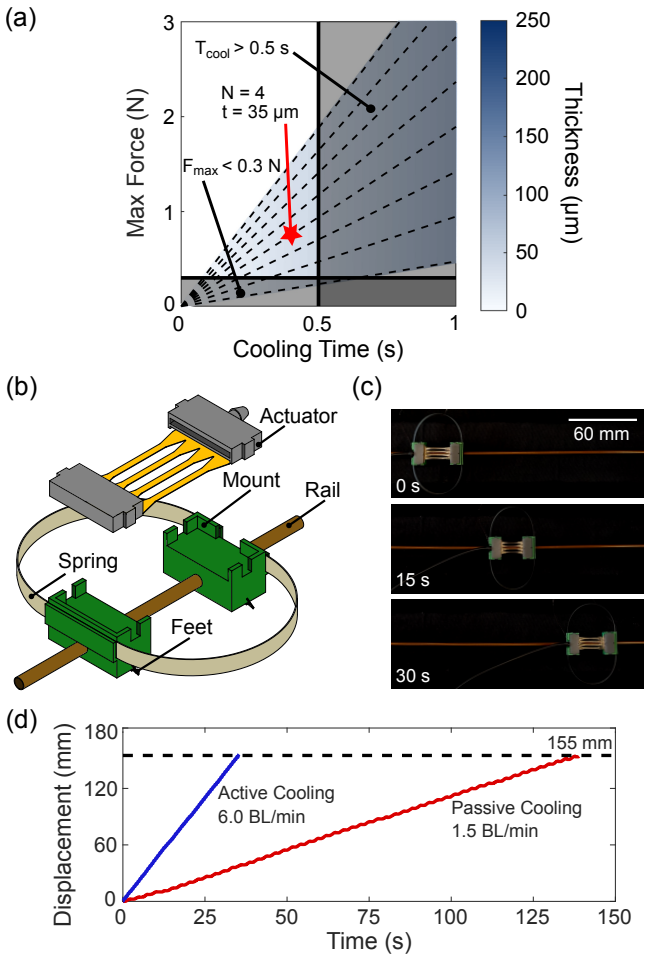

Fig. 6. An inchworm inspired locomotion robot. (a) The design contour used to select the thickness and number of LCE units to integrate into our thermal actuator. (b) Schematic of the proposed inchworm robot. (c) Snapshots of our inchworm robot at different times in the active cooling configuration. (d) Locomotion results of our inchworm robot. Our inchworm robot could achieve a top speed of 6.0 BL/min and 1.5 BL/min in the active and passive cooling configurations, respectively

a compression test using a material tester (ESM750SFG, Mark-10) and digital force gauge (M7-20, Mark-10). We estimated the preload force based on the stiffness of the flexure spring and preload from the LCE units ($F_{load} = 0.0721$ N). Considering LCE units that have a gauge length of 20 mm ($\epsilon = 0.25$), the minimum required blocked force was 0.3 N using Eq. 7. Based on these performance requirements, we used our design contour (see Fig. 6a) and selected to bundle 4 LCE units, each with a thickness of approximately 35 µm. We chose to exceed our estimated force requirement to account for unmodeled friction in our analysis.

2) Robot Locomotion Experiments: We evaluated our robot with both active cooling and passive cooling to quantify the improvements bundling (i.e., increasing the surface area of our actuator) and active cooling (i.e., increasing the convective heat loss coefficient) had on the locomotion speed. For all experiments, we pulsed the LCE units with 6 W for 0.1 seconds, resulting in a maximum temperature of approximately 90°C based on our analytical model, to reduce the time to heat the actuators compared to the experiments in Section III. For the active cooling configuration, we cooled the actuator for

IEEE Robotics and Automation Letters (RA-L) paper, presented at ICRA 2026, Vienna, Austria. Cite as RA-L paper.

0.5 seconds (1.7 Hz gait frequency). We scaled the volumetric flow out of the vent to maintain a flow velocity of 3 m/s due to the wider vent to account for the bundled LCE units.

For the passive cooling configuration, we experimentally determined that a cooling time of 2.5 seconds was acceptable to take into account the reduced cooling efficiency due to bundling LCE units together and to achieve a similar gait length as the active cooling configuration. For both experiments, we measured the position of the robot during post processing using open source tracking software (Tracker).

3) Results: The experimental top speed of our inchworm robot was 6.0 BL/min in the active cooling configuration and 1.5 BL/min in the passive cooling configuration over a distance of 155 mm (see Fig. 6c and Fig. 6d). While the theoretical speed of our robot was over 10 BL/min, we believe that unmodeled friction between the feet of the robot and the ground reduced the stride length, thus reducing our top speed. Nevertheless, compared to existing LCE-driven crawling robots, which have top speeds less than 0.21 BL/min [8]–[12], our inchworm robot was over 25 times faster in the active cooling configuration. While this was expected given that the robots we surveyed relied on passive cooling, our inchworm robot in the passive cooling configuration was still over 7 times faster than existing literature. We attribute this to the increased surface area when bundling several LCE units in parallel that improved the cooling rate of the actuator.

B. Textile Cuff with Integrated Haptic Feedback

Current state-of-the-art wearable haptic interfaces using thermal actuators, such as SMA, have a limited application space because they can require up to 10 seconds to cool [13], [14]. We designed and fabricated a textile-based, wearable cuff that generated skin stretch on the forearm and required only 1 second to cool, thus providing more responsive cutaneous haptic feedback (see Fig. 7).

1) Textile Cuff Design: The cuff consisted of two textile straps that were wrapped around the forearm. We 3D-printed a flat tactor that was added to each strap to contact the skin. The tactor was also attached to a mount that held the actuator to generate skin stretch. Because the LCE units were not directly in contact with the skin and our active cooling method provided effective heat transport, no covering was required to thermally isolate the user from the device.

We aimed to achieve 5 mm of total contraction, corresponding to 2.5 mm of displacement at each tactor to ensure we were well above the detection threshold for skin stretch on the forearm [29], [30]. We also aimed for a cooling time of 1 second to ensure we could generate considerably more responsive haptic feedback compared to existing thermally-actuated haptic interfaces.

Following a similar procedure when designing the actuator for the inchworm robot, we estimated the blocked force, F_b, that the actuator must achieve using Eq. 7. In this case, F_{load} was zero because there was no preload on the skin, k represented the stiffness of the skin on the forearm (approximated as 0.1 N/mm for linear displacements [31]), and δx represented the maximum displacement of the skin at each tactor. Assuming each tactor moved the same amount ($\delta x = 2.5$ mm) and the LCE units have a gauge length of 20 mm ($\epsilon = 0.25$), the necessary blocked force that the actuator must achieve was 0.6 N. Based on our design contour, we bundled four LCE units together, each approximately 60 µm thick (see Fig. 7a and Fig. 7b). We again chose to exceed our blocked force requirement to take into account variations in the stiffness of the skin and the stiffness of the textile cuff that we did not consider in Eq. 7.

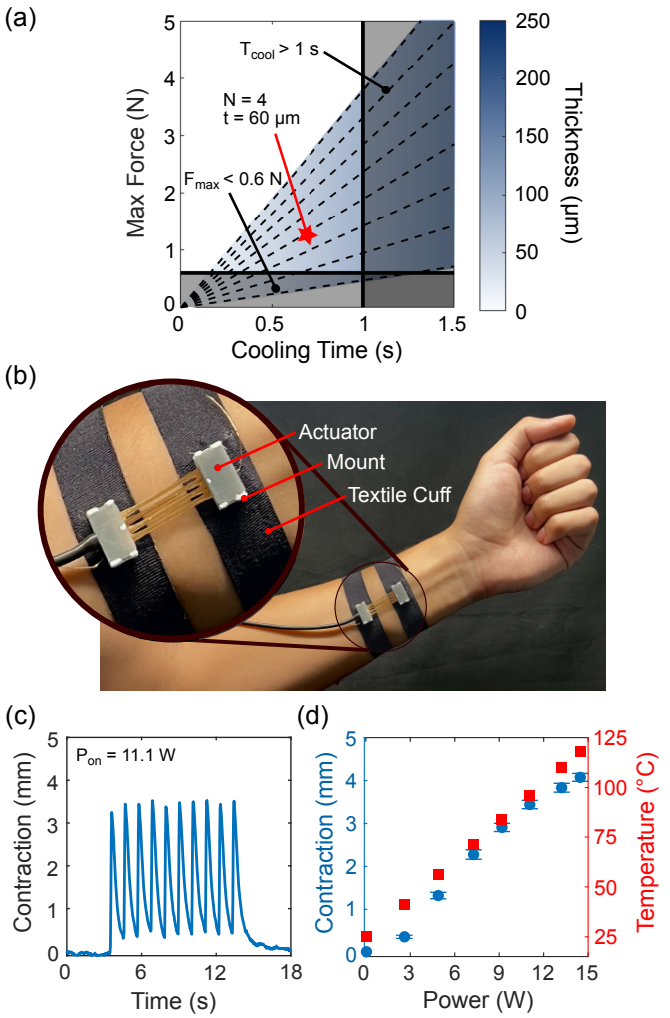

Fig. 7. A textile forearm cuff with integrated haptic feedback. (a) The design contour used to select the thickness and number of LCE units to integrate into our thermal actuator. (b) Example of the haptic device worn on the forearm. (c) Representative results of contraction on the skin when applying 11.1 W during the heating phase. (e) Max contraction of the skin and estimated temperature of the actuator using our analytical model for different power inputs. Different levels of skin stretch can be achieved by varying the input power.

2) Haptic Feedback Experiments: We pulsed the actuator at approximately 0.9 Hz (0.1 seconds heating, 1 second cooling) and measured the contraction of the skin using a camera and open source tracking software (Tracker). We varied the power applied to the actuator from 2.5 W to 14.5 W during the heating phase to achieve varying levels of skin stretch for continuous haptic feedback. For all powers, we estimated the maximum temperature of the LCE units using our analytical model to ensure we were operating within the working limits of our actuator.

3) Results: Our haptic device could generate up to 4 mm of skin stretch by modulating the power applied to the actuator (see Fig. 7c and Fig. 7d). We observed, however, that the actuator was not returning back to its original position (see Fig. 7c). This could be due to a number of reasons, such as non-uniform flow velocity, damping effects due to the compliance of the skin, and the fact that the cooling rate was not defined as the time it takes to go from the max force to zero. Nevertheless, our device was still capable of generating over 3.5 mm of peak-to-peak displacement at 0.9 Hz, which is well above the threshold (0.5 mm) to perceive direction of skin stretch based on existing literature [30].

V. Conclusion

In this work, we developed a new thermally-driven actuator by bundling LCE units in parallel with integrated cooling using forced convection. We presented comprehensive experiments to characterize the trade-off between force output and cooling rate and developed an analytical model to provide guidelines in order to design our actuators for diverse, soft robotic applications. Future work should focus on developing portable electronics for untethered operation and modifying the design contours to take into consideration the power required to heat and cool the actuator for resource-constrained hardware. Future work should also investigate ways to improve the bundling process, such as introducing multiple layers of LCE units to increase the force density and reduce the physical footprint of the actuator.

References

[1] D. Rus and M. T. Tolley, "Design, fabrication and control of soft robots," *Nature*, vol. 521, no. 7553, pp. 467–475, 2015.

[2] B. Mosadegh, P. Polygerinos, C. Keplinger, S. Wennstedt, R. F. Shepherd, U. Gupta, J. Shim, K. Bertoldi, C. J. Walsh, and G. M. Whitesides, "Pneumatic networks for soft robotics that actuate rapidly," *Advanced functional materials*, vol. 24, no. 15, pp. 2163–2170, 2014.

[3] L. Cappello, K. C. Galloway, S. Sanan, D. A. Wagner, R. Granberry, S. Engelhardt, F. L. Haufe, J. D. Peisner, and C. J. Walsh, "Exploiting textile mechanical anisotropy for fabric-based pneumatic actuators," *Soft robotics*, vol. 5, no. 5, pp. 662–674, 2018.

[4] M. Mertmann and G. Vergani, "Design and application of shape memory actuators," *The European Physical Journal Special Topics*, vol. 158, no. 1, pp. 221–230, 2008.

[5] J. Ince, K. Prasad, K. Subhani, A. Duffy, and N. Salim, "Liquid crystalline elastomers as artificial muscles and flexible actuators for robotics/hybrid engineered machinery," *Advanced Composites and Hybrid Materials*, vol. 7, no. 6, pp. 1–41, 2024.

[6] Y.-Y. Xiao, Z.-C. Jiang, X. Tong, and Y. Zhao, "Biomimetic locomotion of electrically powered "janus" soft robots using a liquid crystal polymer," *Advanced Materials*, vol. 31, no. 36, p. 1903452, 2019.

[7] Z. Li, G. Olson, D. K. Patel, L. Yao, and C. Majidi, "Electrically controlled liquid crystal elastomer surfaces for dynamic wrinkling," *Advanced Intelligent Systems*, vol. 6, no. 2, p. 2200402, 2024.

[8] Y. Di, Y. Zhang, Y. Wen, H. Yao, Z. Zhou, Z. Ren, H. Tian, and J. Shao, "Inchworm-inspired soft robot with controllable locomotion based on self-sensing of deformation," *IEEE Robotics and Automation Letters*, 2024.

[9] X. Song, W. Zhang, H. Liu, L. Zhao, Q. Chen, and H. Tian, "3d printing of liquid crystal elastomers-based actuator for an inchworm-inspired crawling soft robot," *Frontiers in Robotics and AI*, vol. 9, p. 889848, 2022.

[10] J. M. Boothby, J. C. Gagnon, E. McDowell, T. Van Volkenburg, L. Currano, and Z. Xia, "An untethered soft robot based on liquid crystal elastomers," *Soft robotics*, vol. 9, no. 1, pp. 154–162, 2022.

[11] H. Yang, X. Yin, C. Zhang, B. Chen, P. Sun, and Y. Xu, "Weaving liquid crystal elastomer fiber actuators for multifunctional soft robotics," *Science Advances*, vol. 11, no. 8, p. eads3058, 2025.

[12] H. S. Choi and D. S. Kim, "Self-repeatable snapping liquid–crystal-elastomer actuator," *Chemical Engineering Journal*, vol. 500, p. 156744, 2024.

[13] N. A.-h. Hamdan, A. Wagner, S. Voelker, J. Steimle, and J. Borchers, "Springlets: Expressive, flexible and silent on-skin tactile interfaces," in *Proceedings of the 2019 CHI Conference on Human Factors in Computing Systems*, 2019, pp. 1–14.

[14] S. Oh, T.-E. Song, M. Mahato, J.-S. Kim, H. Yoo, M.-J. Lee, M. Khan, W.-H. Yeo, and I.-K. Oh, "Easy-to-wear auxetic sma knot-architecture for spatiotemporal and multimodal haptic feedbacks," *Advanced Materials*, vol. 35, no. 47, p. 2304442, 2023.

[15] Q. He, Z. Wang, Y. Wang, Z. Wang, C. Li, R. Annapooranan, J. Zeng, R. Chen, and S. Cai, "Electrospun liquid crystal elastomer microfiber actuator," *Science robotics*, vol. 6, no. 57, p. eabi9704, 2021.

[16] S. Kim and S. Bergbreiter, "Thin-film niti microactuator with a magnetic spring for a tiny launcher mechanism," in *2024 IEEE International Conference on Robotics and Automation (ICRA)*. IEEE, 2024, pp. 13 439–13 445.

[17] Q. He, Z. Wang, Z. Song, and S. Cai, "Bioinspired design of vascular artificial muscle," *Advanced Materials Technologies*, vol. 4, no. 1, p. 1800244, 2019.

[18] J. Jeong, K. Hyeon, J. Han, C. H. Park, S.-Y. Ahn, S.-K. Bok, and K.-U. Kyung, "Wrist assisting soft wearable robot with stretchable coolant vessel integrated sma muscle," *IEEE/ASME Transactions On Mechatronics*, vol. 27, no. 2, pp. 1046–1058, 2021.

[19] J. Jeong, K. Hyeon, S.-Y. Jang, C. Chung, S. Hussain, S.-Y. Ahn, S.-K. Bok, and K.-U. Kyung, "Soft wearable robot with shape memory alloy (sma)-based artificial muscle for assisting with elbow flexion and forearm supination/pronation," *IEEE Robotics and Automation Letters*, vol. 7, no. 3, pp. 6028–6035, 2022.

[20] A. Lara-Quintanilla and H. E. Bersee, "A study on the contraction and cooling times of actively cooled shape memory alloy wires," *Journal of Intelligent Material Systems and Structures*, vol. 27, no. 3, pp. 403–417, 2016.

[21] Y. Wang, Q. He, Z. Wang, S. Zhang, C. Li, Z. Wang, Y.-L. Park, and S. Cai, "Liquid crystal elastomer based dexterous artificial motor unit," *Advanced Materials*, vol. 35, no. 17, p. 2211283, 2023.

[22] X.-T. Nguyen, A. A. Calderón, A. Rigo, Z. G. Joey, and N. O. Pérez-Arancibia, "Smallbug: A 30-mg crawling robot driven by a high-frequency flexible sma microactuator," *IEEE Robotics and Automation Letters*, vol. 5, no. 4, pp. 6796–6803, 2020.

[23] D. Kim, B. Kim, B. Shin, D. Shin, C.-K. Lee, J.-S. Chung, J. Seo, Y.-T. Kim, G. Sung, W. Seo *et al.*, "Actuating compact wearable augmented reality devices by multifunctional artificial muscle," *Nature communications*, vol. 13, no. 1, p. 4155, 2022.

[24] G. Dong, F. Zhao, Z. Gao, and S. Cai, "Liquid crystal elastomer for compression therapy," *Advanced Healthcare Materials*, vol. 14, no. 3, p. 2402881, 2025.

[25] G. Dong, T. Feng, R. Chen, and S. Cai, "Autonomous thermal modulator based on gold film-coated liquid crystal elastsomer," *Advanced Materials Technologies*, vol. 9, no. 20, p. 2400512, 2024.

[26] S. W. Churchill and H. H. Chu, "Correlating equations for laminar and turbulent free convection from a horizontal cylinder," *International journal of heat and mass transfer*, vol. 18, no. 9, pp. 1049–1053, 1975.

[27] S. W. Churchill and M. Bernstein, "A correlating equation for forced convection from gases and liquids to a circular cylinder in crossflow," 1977.

[28] S. M. Mirvakili and I. W. Hunter, "Artificial muscles: Mechanisms, applications, and challenges," *Advanced materials*, vol. 30, no. 6, p. 1704407, 2018.

[29] H. Olausson, I. Hamadeh, P. Pakdel, and U. Norrsell, "Remarkable capacity for perception of the direction of skin pull in man," *Brain research*, vol. 808, no. 1, pp. 120–123, 1998.

[30] N. A. Caswell, R. T. Yardley, M. N. Montandon, and W. R. Provancher, "Design of a forearm-mounted directional skin stretch device," in *2012 IEEE Haptics Symposium (HAPTICS)*. IEEE, 2012, pp. 365–370.

[31] K. Y. J. Bark, *Rotational skin stretch feedback: a new approach to wearable haptic display*. Stanford University, 2009.